Int J Adv Manuf Technol (2010) 50:569–577
DOI 10.1007/s00170-010-2516-7

ORIGINAL ARTICLE

Burr analysis in microgrooving

Duy Le · Jong-Min Lee · Su-Jin Kim · Dong-Yoon Lee · Seok-Woo Lee

Received: 23 July 2009 / Accepted: 4 January 2010 / Published online: 4 March 2010

Abstract Microburr formation affects badly on product's quality, especially the finishing surface. Besides, deburring techniques on microcutting are almost impossible or high cost. Understanding burr formation phenomena and minimizing burr size in correlation with cutting conditions and material properties, in this case, are more appropriate. For the purpose of exploring the burr phenomena in micrometal cutting, two cases of burr formation in grooving micropatterns are introduced in the paper. The burr happens along the cutting direction—side burr—of prism pattern, and the other happens at the exit edge of the pattern in the cutting direction—exit burr—of pyramid pattern. Besides, the exit break off which occurs during the exit burr formation is also studied. The analytical solutions for predicting the burr and break off size in each case are also proposed and compared with experiments.

Keywords Burr formation · Microgrooving · Micropattern · Slip line theory · Hardness

1 Introduction

The motivation for micromanufacturing arises from the translation of the knowledge obtained from the macro-machining domain to microdomain. However, there are challenges and limitations on micromachining, and simple scaling might not be used to model the phenomena of micromachining operations effectively [1]. High-accuracy miniaturized components are increasingly in demand for various industries, such as aerospace, biomedical, electronics, environmental, communications, and automotive. This miniaturization will provide microsystems that promise to enhance health care, quality of life, and economic growth in such applications as microchannels for lab on chips, shape memory alloy "stent", fluid graphite channels for fuel cell applications, subminiature actuators and sensors, and medical devices [2–5].

One of the most popular micromanufacturing methods is microcutting, especially metal cutting, and micropatterns which are applied in most of the applications listed above are fabricated by microgrooving. Burr formation in microgrooving usually ruins the finishing pattern surface. Deburring techniques on those surfaces are almost impossible or too specific, complicated, and high cost [6]. Understanding burr formation phenomena and minimizing burr size in correlation with cutting conditions and material properties, in this case, are more appropriate [7]. But most of previous successful researches are about burr formation in general cutting, so microburr problems still need to be solved in order to serve the requirement of the industry. For the purpose of exploring the burr phenomena in micrometal cutting, two cases of burr formation in turning micropatterns are introduced in the paper. The burr happens along the cutting direction—side burr—of prism pattern, and the one happens at the exit edge of the pattern in the cutting direction—exit burr—of pyramid pattern.

D. Le · J.-M. Lee · S.-J. Kim (✉)
Department of Mechanical Engineering,
Gyeongsang National University,
Gajwa, Jinju, South Korea
e-mail: sujinkim@gnu.ac.kr

D.-Y. Lee · S.-W. Lee
Korea Institute of Industrial Technology,
Ansan, Seoul, South Korea

2 Side burr in grooving microprism pattern

2.1 Cutting model

The cutting model is built from a 200 mm in diameter and 1,000 mm in length roll mold in turning microprism pattern. The idea is taking a small square piece of the roll surface and assuming it is similar to grooving microprism pattern on a plate mold. This will make the first study about side burr happening along the pattern more general as shown in Fig. 1. Cutting material is the copper coated outside the roll. Because the coating technology cannot ensure that everyplace on the roll surface could have the same coating quality, Vickers hardness tests are required to check the material properties of the surface. Then combining with the work of Hirano et al. [8], an approximate relation between Vickers hardness and yield stress could be claimed.

$$h = 2.4 \sim 2.7 S_y \tag{1}$$

where h (kilograms per square millimeter) is Vickers hardness and S_y (newton per square meter) is yield stress of coated copper.

In microgrooving, according to this study, at every cutting depth, there obviously exists a critical thickness t_{cr} at which cutting is impossible. It causes plowing on the pattern's side surface along with the deformed chip formation upon it. In case of the remained thickness of workpiece reaches to t_{cr} value, the top part of the triangle begins to deform plastically along the feed direction. This concept comes from the comparison and evaluation between burr in general cutting [9] and micrometal cutting theory [1].

To determine the critical thickness t_{cr}, a cutting of the infinite plate is considered. As shown in Fig. 2, there is uniform stress distribution along its unit width. This scheme

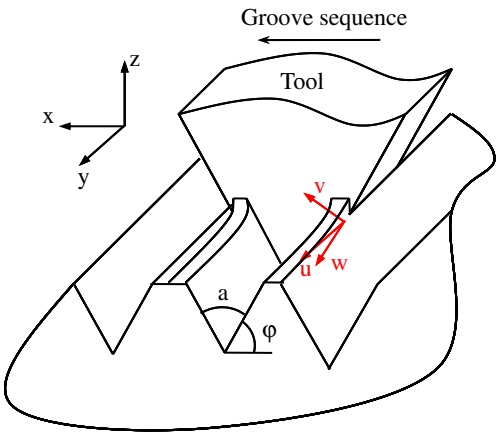

Fig. 1 Prism model

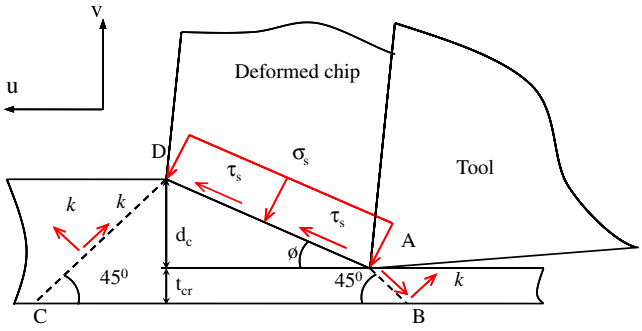

Fig. 2 Determination of the critical thickness t_{cr}

is obtained from the normal cross section of the tool edge, where u-axis is same to y-axis and v-axis is normal to pattern side, in Fig. 1. Nakayama and Arai and Toropov and Ko's experiments [7, 9] have shown that burr formation in the feed direction during turning operation is caused by the stresses in shear plane AD. Due to these stresses, tension is expected in the plate when the thickness is close to t_{cr}. Slip lines AB and DC are the boundaries of the tensile area. Since the exit surface is free from external stresses, the slip lines are inclined to the exit surface at 45°, following theory of plasticity [10, 11]. Besides, this theory implies that the normal and shear stresses on these lines are equal to the value of plasticity k which is determined from Silva's criterion [12] as

$$k = \frac{\sigma_y}{\sqrt{3}} \tag{2}$$

where σ_y can be obtained from Eq. 1. The force balance of element ABCD with respect to the u-axis gives

$$(\tau_s \cos\phi + \sin\phi)\frac{d_c}{\sin\phi} - 4kt_{cr} - 2kd_c = 0 \tag{3}$$

with d_c is undeformed chip thickness and ϕ is shear angle which can be estimated using Merchant's theory

$$\phi = \frac{\pi}{4} + \frac{\alpha}{2} - \frac{\gamma}{2} \tag{4}$$

In which α is rake angle, γ is friction angle which can be obtained by applying Merchant's circle.

$$\gamma = \arctan\left(\frac{F_v + F_u \tan\alpha}{F_u + F_v \tan\alpha}\right) \tag{5}$$

with F_u and F_v can be estimated from F_y and F_z which are already found in previous research [13].

Then from Eq. 2, t_{cr} can be calculated

$$t_{cr} = \frac{d_c(\tau_s \cot\phi + \sigma_s - 2k)}{4k} \tag{6}$$

where $d_c = d_i \sin\frac{a}{2}$, d_i being relative cutting depth. In this case, critical thickness is also called burr thickness.

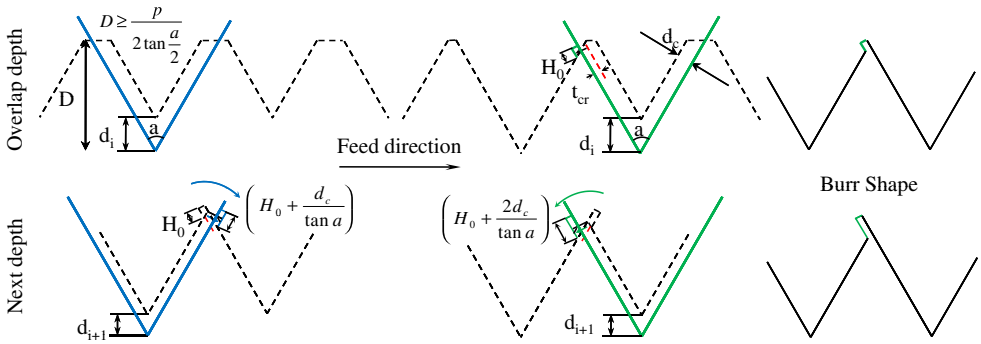

Fig. 3 Continuous side burr formation

2.2 Continuous side burr formation

Burr happens at each cutting depth of the grooving schedule, according to the cutting condition. So burr should be counted at each cutting step to form the final burr size, but according to Fig. 3, after some depths, burr counting should be started from the overlapped depth at which burr is called initial burr. The overlapped depth is considered when the groove width is equal or greater than the designed pitch.

$$D \geq \frac{p}{2\tan\frac{a}{2}} \tag{7}$$

where D is total depth at step n; p and a are pitch and angle of pattern, respectively. Initial burr might develop continuously to the final depth to form final burr as Fig. 3.

This model is applied for the case in which burr is fully formed without fracture. Starting from the overlapped cutting depth, the micro plate material of critical thickness is shifted perpendicular to the tool edge to form the initial burr.

$$H_0 = \frac{2t_{cr}}{\tan a} \tag{8}$$

At the step next to overlapped depth, the initial burr is rotated around the tip of the triangle due to the radius effect of the cutting edge in microcutting, and the material at the bottom of the initial burr is again shifted perpendicular to the tool edge. Those two phenomena happened at once to form the continuous burr. So far from the next steps, burr is formed continuously as described till the last step.

$$H_m = H_0 + \sum_{i=n+1}^{m} \frac{2\left(d_i \sin\frac{a}{2}\right)}{\tan a \sin\frac{a}{2}} \tag{9}$$

which is final burr height.

2.3 Discontinuous side burr formation

Considering again about the grooving step after the initial burr formed, for general material, there will be two cases of burr formation. First is continuous burr formation as described above. Second is discontinuous burr formation which will be further discussed in this section. As observing Fig. 3, discontinuous in this case means after the overlapped depth burr of the previous depth will be cut off at the next depth. According to Nakayama and Arai's experiments on brass in general cutting [7], when shear strain is greater than three (γ>3), the deformation is accompanied by side flow which causes the side burr. This is the condition about plastic deformation ability of material. In the case of this study, even when the plastic deformation that needs for side burr to develop continu-

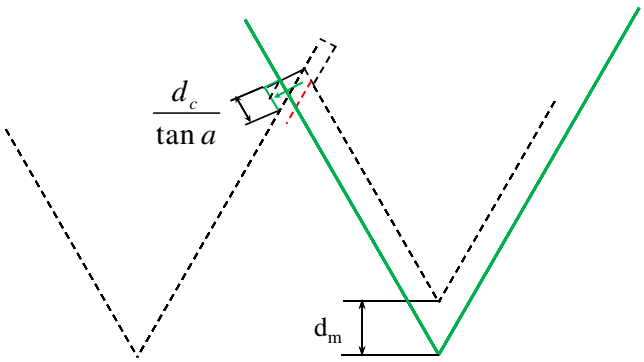

Fig. 4 Side burr formation at final depth

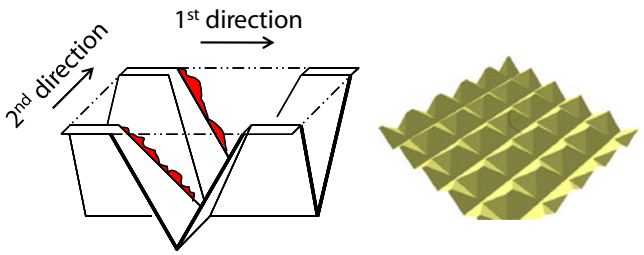

Fig. 5 Pyramid model

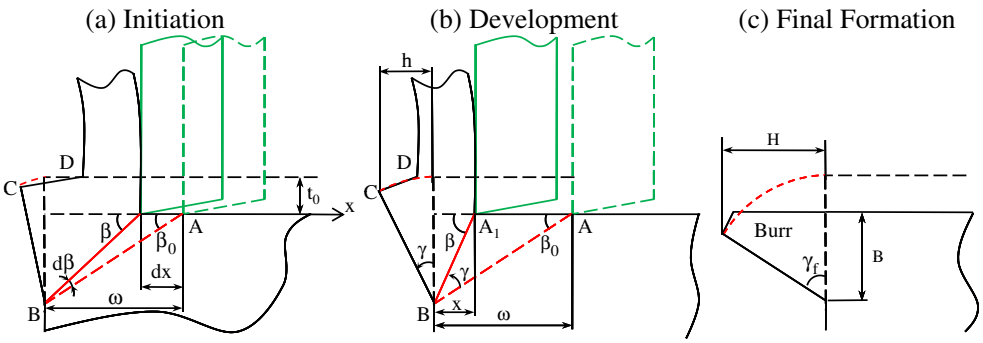

Fig. 6 Exit burr formation

ously is higher than that, it is acceptable to analyze the discontinuous case with this condition. In this case, shear strain is estimated as always less than three ($\gamma<3$). It means that burr from the previous cutting depth is always removed at the next depth or the burr size of the scheduled grooving is burr size of the final cutting depth

$$H = \frac{2t_{cr}}{\tan a} \tag{10}$$

which is shown in Fig. 4.

3 Exit burr and break off in grooving micropyramid pattern

3.1 Cutting model

Pyramid pattern can be formed in the sequence of first groove to create prism pattern and the second groove which is orthogonal with the first one. During the second groove each time when tool moves across one prism pattern, there is exit burr or break off at the edge as shown in Fig. 5. In this case, rake angle is zero so that exit burr happens in orthogonal cutting. Taking a cross section in the pattern as Fig. 6 allows exploring the cutting process and exit burr phenomenon.

Exit burr mechanism can be divided into three parts based on the observation from the machining tests on plasticine [14]. Initiation: As the tool approaches the end of the workpiece, there is a transition point at which the chip formation stops and plastic deformation below the machined surface, along cutting direction, begins. Initiation of burr formation is characterized by the initial negative shear angle β_0 and initial distance of tool tip ω. An interesting point is that the initial negative shear angle, β_0, is almost 20° regardless of the workpiece material and the cutting conditions, when exit angle is 90°. This has been verified by previous researchers [14, 15]. Development: As the tool move forward after initiation from A to A_1, negative shear plane also rotates from BA to BA_1. Once the initial negative shear plane is formed, the final point of the negative shear plane which crosses the exit surface of the prism pattern at point B in Fig. 6 will act as plastic hinge and not translate during the burr development. Formation: Finally, the burr is formed with or without fracture because of increasing strain along the negative shear plane as the tool approaching the end of workpiece. If fracture occurs along the negative shear plane or through existing burr, it will remove or reduce the burr.

3.2 Exit burr formation without break off

In the first stage of studying the exit burr of micropyramid pattern, it is recommended to apply the model about exit burr in general cutting model of [15] following the cutting

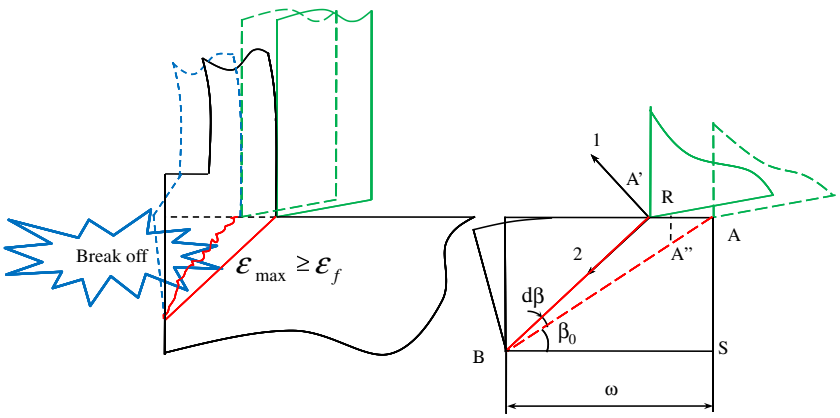

Fig. 7 Exit break off model

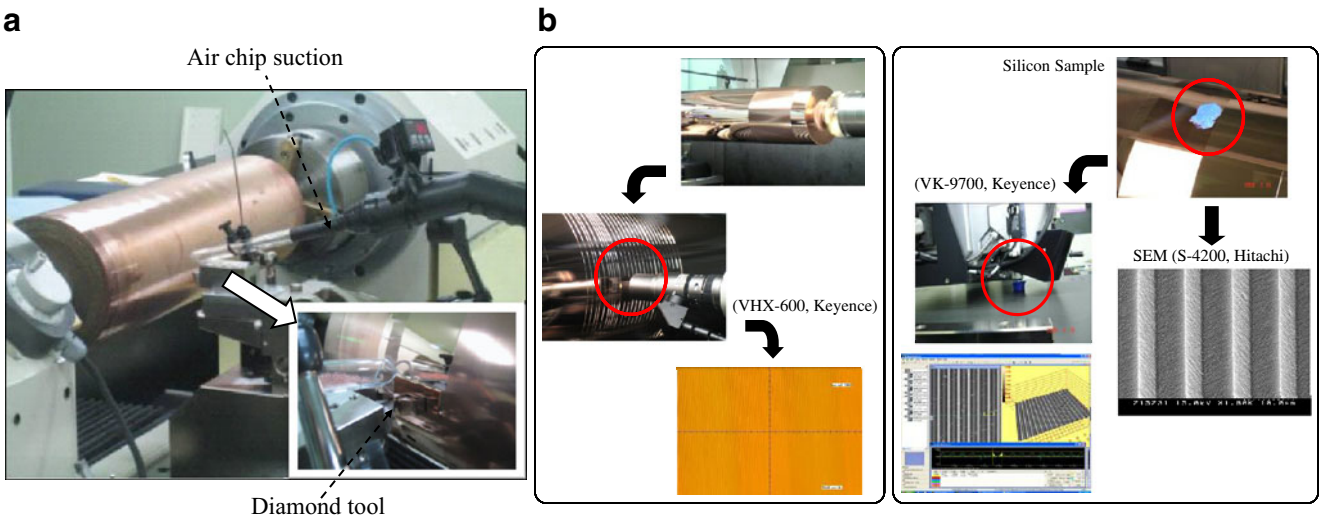

Fig. 8 Experiment setup. **a** Turning copper mold with diamond tool and chip suction. **b** Capturing pattern with digital microscope and SEM

schedule of the second groove. At each depth, initial length is also assumed as burr thickness and can be obtained as

$$\omega = \frac{k_s\left(d_c \frac{1}{\sin\phi} + sL\sin\phi\right)}{\cos\phi\left(\frac{k_0}{2}\cos^2\beta_0 + \frac{S_y}{4}\tan\beta_0\right)} \tag{11}$$

with k_0 is the yield shear strain obtained by Mise's criterion, k_s is shear yield strength in shear zone, L is tool chip contact length, and burr size can be obtained geometrically from Fig. 6 by

$$B = \omega\tan\beta_0 \tag{12}$$

$$H = (d_c + B)\sin\gamma_f \tag{13}$$

which B and H are burr thickness and burr height, respectively.

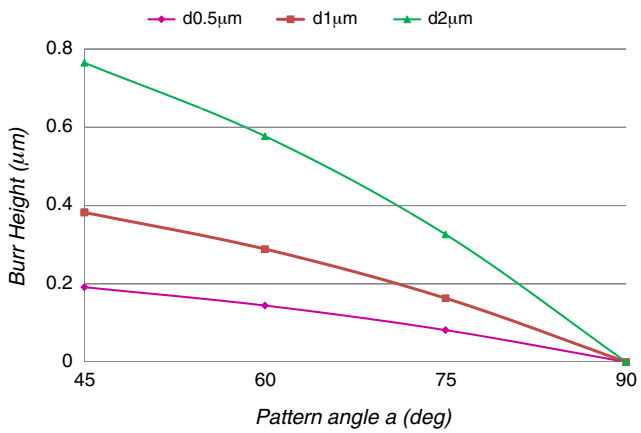

Fig. 9 Burr height in different pattern angles with different final depths

3.3 Exit break off during burr formation

Beside the burr development, edge break off during burr formation greatly affects the product quality. If edge breakout occurs instead of burr formation, a crack along the negative shear plane will be initiated. It depends on the material behavior, particularly the fracture strain in this case. A fracture criterion is necessary for predicting the occurrence of fracture during burr formation. While the criteria for initial yielding and brittle fracture require only the current state of stress, a behavior of the ductile material is not clearly defined due to the extent of the plastic deformation that can occur before fracture happens: The behavior depends on the deformation history in the ductile material. The behavior of most materials is practically

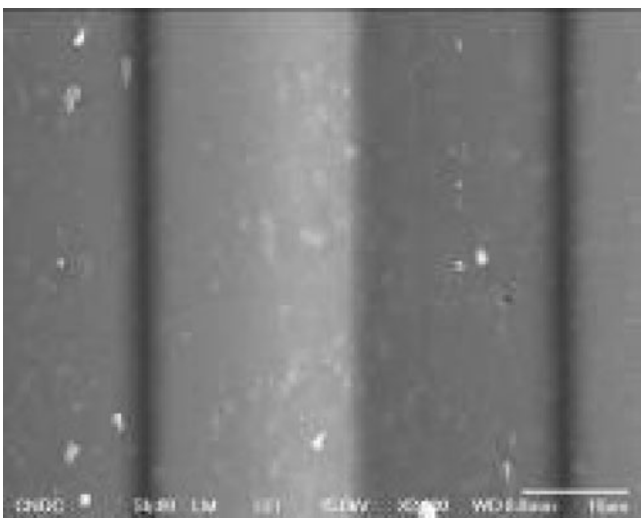

Fig. 10 Ninety-degree prism pattern

Table 1 Single grooving, depth = pitch, V 80°, 210 Hv

Depth / v_c	5 m	10 m	15 m
200 m/min	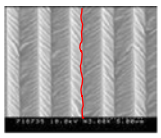	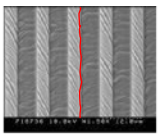	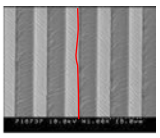
Burr	0.23 m	0.48 m	0.57 m
300 m/min	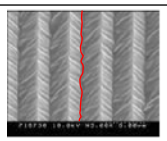	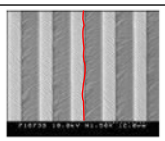	
Burr	0.27 m	0.45 m	0.53 m
400 m/min	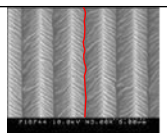	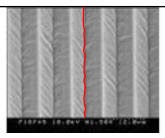	
Burr	0.25 m	0.5 m	0.55 m

located between two extreme cases: a fully ductile material and a perfectly brittle material which fracture without plastic deformation, like crystal. In a ductile material such as copper which large plastic deformation occurs before fracture, it is not convenient to decide the fracture condition by using stress state of the workpiece. It is suggested to use strain instead of stress to apply with the fracture criterion. Even in coated copper, a less ductile material which is accompanied by less plastic deformation before fracture, the ductile fracture criterion by McClintock is assumed to be applied. Applying McClintock's criterion, Ko and Dornfeld's work [15] shows that with pure copper using strain hardening index 0.54 gives fracture strain in exit burr formation ε_f=2.11, and according to the work of Lin [16], the fracture strain ε_f of copper alloy is 1.2. So its suitable for applying fracture strain ε_f=1.2 in this study. The strain at the initial point is zero and increases almost linearly as the negative shear angle increases. So by monitoring the maximum shear strain of the area under grooved surface, fracture can be detected. If the maximum strain is greater than the fracture strain then fracture happens.

$$\varepsilon_{max} \geq \varepsilon_f \tag{14}$$

The maximum shear strain, ε_{max}, here can be approximated as the strain at the tool tip in Fig. 7, and it can be obtained as

$$\bar{\varepsilon}_{tooltip} = \varepsilon_{max} = \int_{\beta_0}^{\beta} \left(\frac{\sqrt{2}}{3} \sqrt{\frac{6}{\beta^2} + \frac{3}{2\tan^4\beta}} \right) d\beta \tag{15}$$

4 Experiment and results

Roll mold was coated with copper and grooved on a precise turning center, as shown in Fig. 8, with single crystal diamond (SCD) tool V shape 60°, 80°, and 90°; hardness is within the range of 210 to 270 Hv. First groove formed prism pattern and second groove formed pyramid pattern. Test cases were also done following that sequence and captured results by digital microscope (Keyence VHX-600 and VK-9700) and SEM (Hitachi S-4200).

4.1 Prism pattern

Figure 9 shows the relation of burr height and pattern angle in cases of final cutting depths are 0.5, 1, and 2 μm. According to the prediction, burr height grows proportionally to the angle decrement and also the increment of depth, and this satisfies the previous experimental works of Nakayama and Arai about general burr [7]. Test cases are taken with SCD tool V shape 60°, 80°, and 90°; cutting speed v_c 200, 300, and 400 m/min; single and multiple grooving. Theoretically, there is no burr when the pattern angle reaches to 90° as test case in Fig. 10, but in other experimental conditions somehow show that burr still happens.

Table 1 shows the surface result after grooving with single depth equal pitch, SCD tool V shape angle 80°, and workpiece hardness 210 Hv. Table 2 shows the results after grooving with two depths, cutting speed 300 m/min, and workpiece hardness 210 Hv. Observing the surface of prism

Table 2 Two-step grooving, 300 m/min, 210 Hv

Depth / Angle	10+5 m
80° (pitch = 15 m)	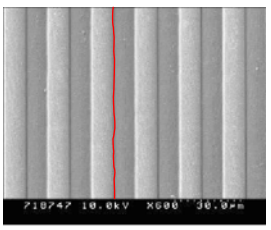
Burr	0.3 m
60° (pitch = 13.02 m)	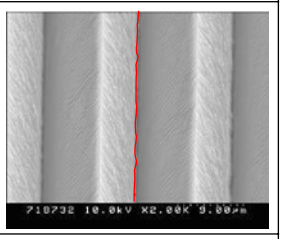
Burr	0.75 m

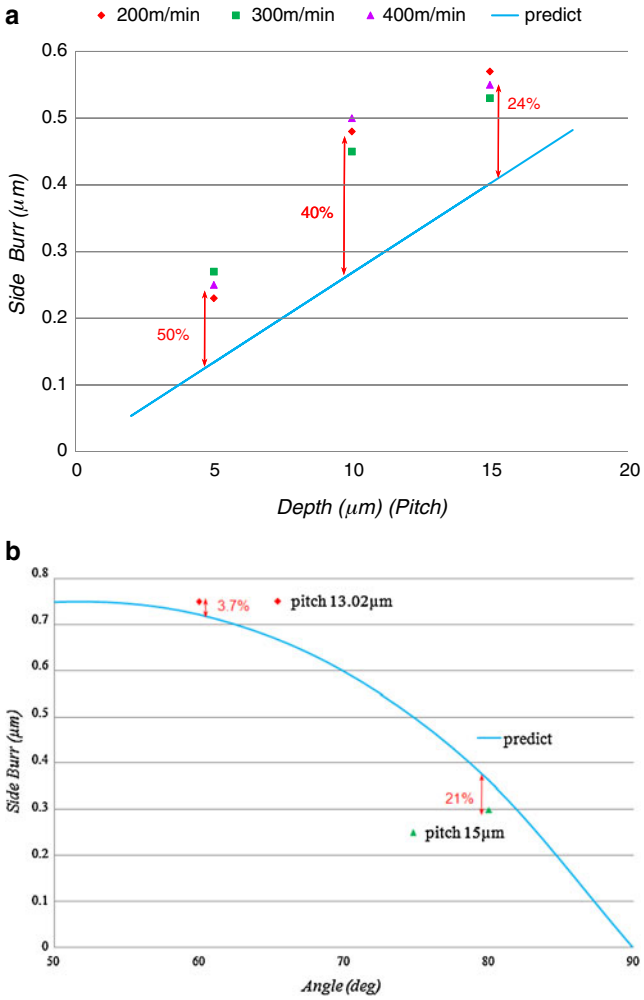

Fig. 11 Comparison between prediction and experiment on side burr of prism pattern. **a** Single grooving, depth = pitch, *V* 80°, 210 Hv. **b** Two-step grooving, 300 m/min, 210 Hv

pattern from above, wavy lines at the top of patterns which are shaped by side burr can be seen clearly. In order to compare the results with the prediction, an orthographic projection of burr height in Eq. 10 is taken.

$$\text{side burr} = H \sin\left(\frac{a}{2}\right) \tag{16}$$

Figure 11 gives the comparison between prediction and result from Table 1 to Table 2 of side burr. For single groove, max error is 50% and min is 24%. For two-step grooving, max error is 21% and min is 3.7%.

4.2 Pyramid pattern

Some predicted results for exit burr of pyramid pattern shown in Fig. 12 conclude that exit burr size grows proportionally to the decrement of hardness and also the increment of cutting depth. In the relation with pattern

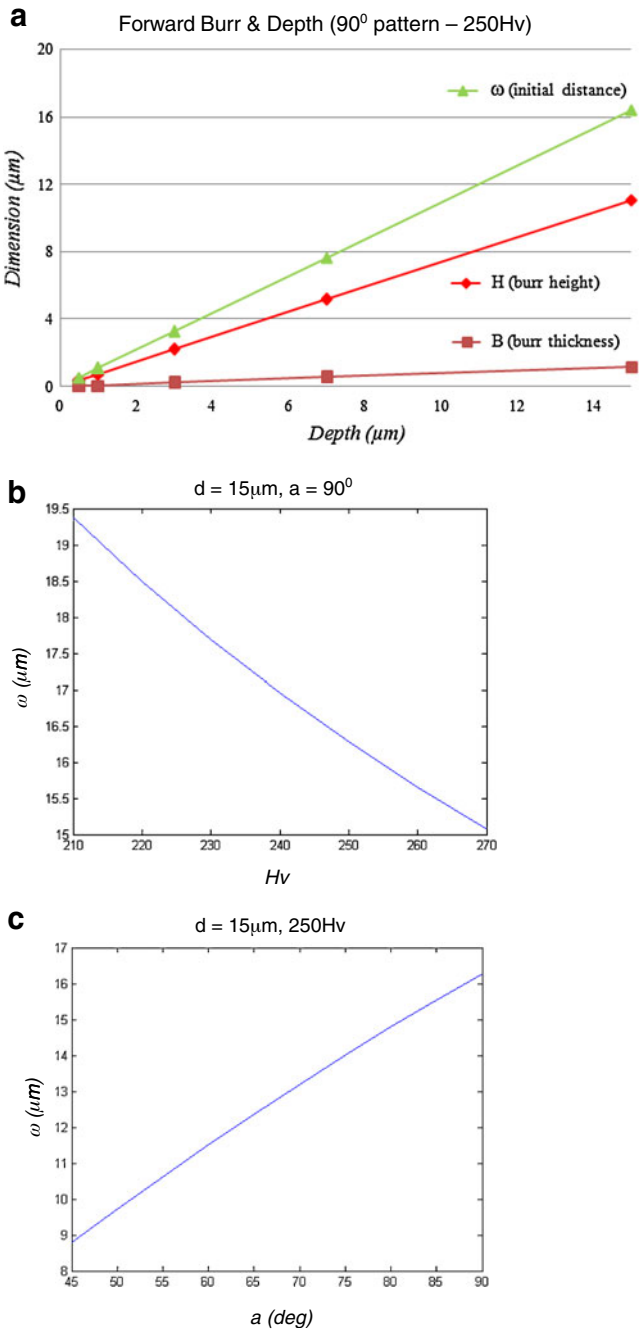

Fig. 12 Predicted results on exit burr of pyramid pattern. **a** Exit burr and cutting depth, *V* 90°, 250 Hv. **b** Initial distance and Hv. **c** Initial distance and pattern angle

angle, burr size increases when angle increase, against the rule in side burr of prism pattern. The reason comes from the geometry of the cutting model, as angle increases then cutting depth on the side wall of the pyramid increases so that burr size increases. Those predictions agree with the rules about burr formation in general cutting with previous researches [7, 14, 15].

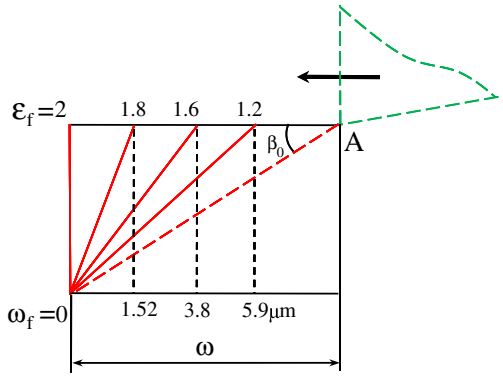

Fig. 13 Relation of exit break off and fracture strain ε_f

By the way, in this study, the main results from the experiments are about the exit break off which are also taken place during the exit burr formation. Test cases are taken with SCD tool *V* shape angle 90° in case of single grooving. Cutting speed for second groove is separated into two groups: high speed 300 m/min with second groove follows turning direction, and low speed 10, 6, and 5 m/min with second groove follows feed direction, as shown in Fig. 14. The relation of exit break off size, shape, and fracture strain is predicted as Fig. 13.

Figure 14 shows the comparison between prediction and experiment on exit break off in grooving pyramid pattern. The predicted result for this case gives break off size 5.97 μm at negative shear angle 45° as Fig. 14a. The measured results from experiments with cutting speed at 300 and 10 m/min give the break off size 7.5 and 6 μm (Fig. 14b, c).

5 Conclusion

Microburr mechanism in grooving prism and pyramid pattern was investigated according to previous burr researches. Methods of predicting side burr in prism pattern and exit break off in pyramid pattern were suggested. Grooving prism and pyramid pattern on roll mold with *V* shape SCD tool, measuring finished surface in 2D and 3D, were setup to check with the predicted results. In prism pattern, new concept of continuous and discontinuous burr development through scheduled grooving was proposed. Equation 6 shows the critical thickness where the cutting is impossible, or it can be called side burr thickness. Equations 9 and 10 give the total side burr height and burr height at final depth, respectively. The errors from the predicted and experimental results in case of two-step grooving are less than 21%. In pyramid pattern, exit burr thickness and height can be found by Eqs. 12 and 13, but more importantly, material break off model was applied into grooving pyramid pattern. Exit break off is predicted by comparing the max shear strain ε_{max} along the negative shear plane, which is found by Eq. 15, with the fracture strain ε_f of coated copper, and the errors of predicted exit break off compared to experiments are less than 14.7%. The gap could be caused by lacking of cutting velocity effect on the burr formation model while there are several cutting speeds in the experiments.

The burr formation process is quite complex in general and macro size and even more complicated in microcutting. This work attempts to develop a new research field about microburr formation in microgrooving which is widely used in nowadays industry, especially light transmission industry. Further work might worth to be carried out for the requirement of higher quality micropattern.

Acknowledgement The authors wish to acknowledge the Ministry of Knowledge Economy of South Korea for supporting this work.

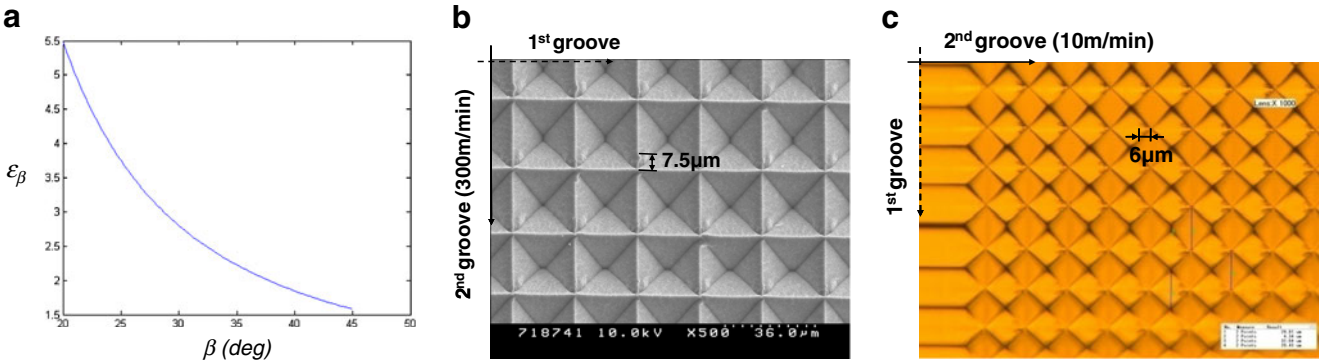

Fig. 14 Comparison between prediction and experiment on exit break off in pyramid pattern. **a** Prediction of β till break off occur with ε_f=1.2. **b** Break off size with v_c=300 m/min. **c** Break off size with v_c=10 m/min

References

1. Chae TJ, Park SS, Freiheit T (2006) Investigation of micro-cutting operations. Int J Mach Tools Manuf 46:313–332
2. Lang W (1999) Reflexions on the future of microsystems. Sens Actuators A 72:1–15
3. Madou MJ (ed) (2002) Fundamentals of microfabrication: the science of miniaturization (2nd edn). CRC, Boca Raton
4. Corbett J, McKeon PA, Peggs GN (2009) Nanotechnology: international developments and emerging products. CIRP Ann 49:523–546
5. Weck M, Fischer S, Vos M (1997) Fabrication of micro components using ultra precision machine tools. Nanotechnol 8:145–148
6. Schaller T, Bohn L, Mayer J, Schubert K (1999) Microstructure grooves with a width of less than 50 μm cut with ground hard metal micro end mills. Precis Eng 23:229–235
7. Nakayama K, Arai M (1987) Burr formation in metal cutting. CIRP Ann 36:33–36
8. Hirano A, Sakane M, Hamada N (2007) Relationship between Vickers hardness and inelastic material constants. J Soc Mater Sci 56(5):445–452
9. Toropov A, Ko SL (2005) A model of burr formation in the feed direction in turning. Int J Mach Tools Manuf 46:1913–1920
10. Astakhov VP (ed) (1999) Metal cutting mechanics. CRC, Boca Raton
11. Chakrabarty J (ed) (1987) Theory of plasticity. McGraw-Hill, New York. ISBN-10:0071001638
12. Silva VD (ed) Mechanics and strength of materials. Springer, Berlin
13. Lee JM, Le D, Kim SJ, Lee SW, Chae TJ (2009) Development of micro pattern cutting simulation software. Trans KSME A 33:218–223. doi:10.3795/KSME-A.2009.33.3.218
14. Ko SL, Dornfeld DA (1991) A study on burr formation mechanism. J Eng Mater Technol 113:75–87
15. Ko SL, Dornfeld DA (1996) Analysis of fracture in burr formation at the exit stage of metal cutting. J Mater Process Technol 58:189–200
16. Lin ZC, Lin YY (2001) Three-dimensional elastic–plastic finite element analysis for orthogonal cutting with discontinuous chip of 6-4 brass. Theor Appl Fract Mech 35:137–153